Multi-Frequency Upper Mid-Band Localization

Tomer Raviv, Seongjoon Kang, Marco Mezzavilla, Sundeep Rangan, and Nir Shlezinger

Abstract—The upper mid-band, often referred to as FR3, embodies an attractive balance of coverage and spectrum availability. As such, it is envisioned to be a pivotal band for future wireless communication, whose unique characteristics also offer enticing opportunities for RF localization. In this context, the lower FR3 band provides great range but limited resolution due to smaller bandwidth and antenna array size; conversely, higher FR3 frequencies are limited in range due to pronounced path loss attenuation, but offer wider bandwidth and larger antenna counts, which result in greater resolution. This paper explores user localization in an uplink scenario, leveraging multiple subbands within FR3 to reduce the localization root mean squared error (RMSE) as compared to localization performed using a single sub-band. We introduce a novel FR3 beamformer that capitalizes on the different analog front-ends and spectral behavior associated with each sub-band. The efficiency of our scheme is evaluated for localization in a challenging urban scenario depicting the heavily clustered NYC Herald Square.

Index terms— Upper Mid-Band, FR3, RF Localization.

I. Introduction

Localization is a vital component in many emerging applications including Internet of Things [1] and autonomous driving [2], [3]. Cellular localization based on radio frequency (RF) signalling [4] provides an attractive method due to the wide coverage and ability to leverage existing devices. highly accurate localization, as node identification within a distributed network is mandatory. A candidate approach to achieve such accurate localization utilizes RF signalling [4].

The selection of the spectrum for RF localization is critical. On the one hand, localization with the high frequency bands including millimeter wave (mmWave) [5] and the TeraHertz (THz) spectra [6] offers high temporal and angular resolution due to the wide bandwidths and large numbers of antenna elements. However, these signals may be limited in range due to high penetration losses [7] and their susceptibility to blockage. The limited range is particularly challenging in cellular localization that often requires visibility to multiple base stations for triangulation. Higher frequencies also suffer from beam split [8], spatial wideband effects [9], and challenges associated with efficient hardware implementation of such transceivers. In contrast, traditional sub-6 GHz offers greater range, but limited spatial and temporal resolution.

The upper mid-band [10], commonly referred to as FR3, spanning approximately from 7GHz to 24GHz, has attracted growing interest for cellular data services due to the balance of coverage and bandwidth. These characteristics also provide

This project has received funding from the Israeli Innovation Authority. T. Raviv and N. Shlezinger are with the School of ECE, Ben-Gurion University of the Negev, Beer-Sheva, Israel (e-mail: tomerraviv95@gmail.com, nirshl@bgu.ac.il). S. Kang, M. Mezzavilla and S. Rangan are with the New York University Tandon School of Engineering, Brooklyn, NY 11201, USA (e-mail: {sk8053, mezzavilla, srangan}@nyu.edu).



Fig. 1: 3D model of the NYC area (Herald Square) used for ray-tracing in [10]. The model provides a fairly accurate mapping of foliage and building materials.

a potential valuable frequency range for localization. Systems that can operate across the entire band can potentially exploit the favorable coverage in the lower bands while utilizing the improve temporal and frequency resolution of the upper components of the bands. The board goal of this paper is to understand how to exploit multiple frequencies in the upper mid-band *simultaneously*.

Upper-Mid Band and RF Localization Background

Initial studies of the FR3 band have mostly focused on communications and channel modeling including frequency characteristics [11], multiple-input multiple-output (MIMO) schemes [12], cellular capacity [10], and coexistence capabilities of cellular services alongside satellite incumbents within this band [13]. Despite this recent progress, the literature thus far has not explored the FR3 band in the context of localization, and particularly the ability to leverage FR3 transceivers that can simultaneously utilize *multiple sub-bands* with possibly *multiple antenna arrays* to facilitate reliable localization.

Various approaches were proposed for localizing from RF signals [1]–[3]. Arguably the most common RF localization approach follows a two-stage methodology [4], [14]: Initially, the received signals are processed to estimate certain physical parameters, e.g., the time of arrival (TOA), which is directly related to the distance between the base station (BS) and the user equipment (UE), or the angle of arrival (AOA), which measures the incident angles. The second stage includes the computation of the UE's spatial coordinates based on these measurements. Alternative RF localization approaches explore direct localization from the signal waveform, particularly in

MIMO settings [15], [16]. These existing works typically focus on localization based on a single observed band.

Multi-frequency localization employing concurrent transmissions over multiple frequencies (though not in the FR3 band), has been explored in several studies [17]-[19]. For instance, [17] constructed a propagation map based on power measurements in different Wi-Fi frequencies, while in [18], the indoor power map is modelled with a multi-frequency Gaussian process. The work [19] exploits multiple bands for high-resolution delay estimation in multipath environments. The above works either focused on indoor or outdoor scenarios based on the chosen frequency band, and thus do not naturally extend to localizing in the FR3 band and its possible usage of multiple antenna arrays for different bands.

Main Contributions

This work aims to bridge the gap for multi-frequency localization in the FR3 band. We propose a FR3 beamformer that selects the spectrum peak from all the available peaks in a multi-band scenario, exploiting the multipath separability of the higher sub-bands within FR3 and the favorable propagation of the lower sub-bands. This, in turn, is translated into robust estimation of the UE's direction and distance, as compared to estimating using each sub-band separately. Our main contributions are summarized as follows:

- Multi-frequency localization scheme: We propose a novel parameter estimation stage as part of the two stage localization pipeline, utilizing multiple sub-bands.
- Simulation in the upper-mid band: The method is validated in the upper mid-band densely clustered urban area with detailed ray-tracing (see Fig. 1). To the best of our knowledge, this work is the first to consider localization for a practical upper-mid band scenario based on ray-tracing simulations. Our simulations demonstrate significant gains of taking into account the widely varying propagation properties of the upper-mid frequencies in RF localization.

The rest of this paper is organized as follows: Section II presents a model for RF localization in the FR3 band; Our proposed scheme is formulated and evaluated in Sections III-IV, respectively, while Section V provides concluding remarks.

II. SYSTEM MODEL

In this section, we present the system model. We first describe the uplink channel model in Subsection II-A, and generalize it to multiple sub-bands in Subsection II-B. Then, we formulate the localization problem in Subsection II-C.

A. Single Sub-band Multipath Uplink Channel

We consider a synchronized BS-UE pair. The BS is located at $p_{BS} = [p_{BS,x}, p_{BS,y}]$, and the UE device is located at $p_{\text{UE}} = [p_{\text{UE},x}, p_{\text{UE},y}]$, both defined in a 2D Cartesian reference system. Localization of the UE is based on uplink orthogonal frequency division multiplexing (OFDM) transmission, with T pilot snapshots and a sufficiently lengthy cyclic prefix (such that the inter-symbol interference is negligible). We denote the carrier frequency, bandwidth and number of subcarriers of the OFDM system by f, B and Q, respectively. The UE is equipped with a single antenna, while the BS is equipped with M antennas for uniform linear array (ULA).

In this sub-band, we adopt a multipath channel model with L different resolvable propagation paths. Thus, the frequencydomain response for the q-th subcarrier and the m-th ($m \in$ $\{0,\ldots,M-1\}$) antenna element can be written as

$$H_{m,q} = \sum_{l=1}^{L} \alpha_l \cdot e^{-2\pi j f_q \tau_l} e^{-2\pi j df m sin(\theta_l)/c}, \qquad (1)$$

where α_l , τ_l and θ_l denote the *l*-th paths' channel gain, TOA and AOA, respectively. In (1), d is the array spacing, and we use the abbreviated notation $f_q \triangleq f + q \frac{B}{Q}$. Note that for the line of sight (LOS) path l = 1, the TOA and AOA are related to the relative BS-UE locations via

$$\tau(\boldsymbol{p}_{\mathrm{BS}}, \boldsymbol{p}_{\mathrm{UE}}) = \frac{\|\boldsymbol{p}_{\mathrm{BS}} - \boldsymbol{p}_{\mathrm{UE}}\|}{c}$$
(2a)

$$\tau(\boldsymbol{p}_{\mathrm{BS}}, \boldsymbol{p}_{\mathrm{UE}}) = \frac{\|\boldsymbol{p}_{\mathrm{BS}} - \boldsymbol{p}_{\mathrm{UE}}\|}{c}$$
(2a)
$$\theta(\boldsymbol{p}_{\mathrm{BS}}, \boldsymbol{p}_{\mathrm{UE}}) = \arctan\left(\frac{p_{\mathrm{BS},y} - p_{\mathrm{UE},y}}{p_{\mathrm{BS},x} - p_{\mathrm{UE},x}}\right).$$
(2b)

To estimate the user's location at the BS, the user transmits T pilot symbols $\{s_t\}_{t=1}^T$, each symbol $s_t \in \mathbb{S}^Q$, where \mathbb{S} denotes the constellation. The elements of the corresponding observations matrix $\boldsymbol{Y}_t \in \mathbb{C}^{M \times Q}$ at the BS are given by

$$Y_{t,m,q} = H_{t,m,q} s_{t,q} + w,$$
 (3)

where the elements $H_{t,m,q}$ of the channel matrix $oldsymbol{H}_t \in \mathbb{C}^{M imes Q}$ follow (1), and $w \in \mathbb{C}$ is a complex Gaussian noise. Note that, as in [20], H_t can be alternatively formulated as:

$$\boldsymbol{H}_t = \sum_{l=1}^{L} \alpha_l \boldsymbol{a}^M(\theta_l) \circ \boldsymbol{a}^Q(\tau_l), \tag{4}$$

where $\boldsymbol{a}^{M}(\theta) \in \mathbb{C}^{M}$ and $\boldsymbol{a}^{Q}(\tau) \in \mathbb{C}^{Q}$ are the steering vectors formed by $e^{-2\pi j df m \sin(\theta_{l})/c}$ and $e^{-2\pi j f_{q} \tau_{l}}$, respectively.

B. Multiple Sub-bands FR3 Model

We extend the above uplink formulation to simultaneous transmission over K sub-bands within the upper mid-band. The k-th sub-band, $k \in \{1, \dots, K\}$, has carrier frequency $f^{(k)}$, bandwidth $B^{(k)}$ and number of subcarriers $Q^{(k)}$. The resulting system employs multiple sub-bands, each employing a different OFDM signaling with $T^{(k)}$ pilots. Moreover, the BS possesses a different analog front-end for each band, with $M^{(k)}$ being the number of antenna elements of sub-band k. Note that for increasing carrier frequencies $f^{(1)} < f^{(2)} <$ $\dots < f^{(K)}$, the number of antennas typically also increases $M^{(1)} \leq M^{(2)} \leq \ldots \leq M^{(K)}$, resulting in higher angular resolution. In each sub-band, the channel observation follows the model of (3), which is now written as

$$Y_{t,m,q}^{(k)} = H_{t,m,q}^{(k)} s_{t,q}^{(k)} + w^{(k)}$$
(5)

Here, the matrices $\boldsymbol{Y}_t^{(k)}$ and $\boldsymbol{H}_t^{(k)}$ have size $M^{(k)} \times Q^{(k)}$, and the number of pilots satisfies $T^{(k)} > M^{(k)} \cdot Q^{(k)}$.

Algorithm 1: Single Sub-Band Beamformer

Input: Single sub-band samples $\{Y_t\}_{t=1}^T$ **Output:** Estimated spectrum peak $(\hat{\theta}_1, \hat{\tau}_1)$

1 Single Sub-Band Beamformer

- 2 calculate spectrum $P(\theta, \tau)$ by (7)
- identify the peak $(\hat{\theta}_1, \hat{\tau}_1)$ by (9)
 - return $(\hat{\theta}_1, \hat{\tau}_1)$

C. Problem Formulation

We focus on generic two-stage localization [4], [14]. To localize the UE, the BS first estimates the LOS parameters $(\hat{\theta}_1, \hat{\tau}_1)$ using the channel observations $\{\boldsymbol{Y}_t^{(k)}\}_{t=1}^T$ over all sub-bands $k \in \{1, \ldots, K\}$. Then, to estimate the UE location $\hat{\boldsymbol{p}}_{\mathrm{UE}}$, the BS solves a non-linear least-squares problem that aims to minimize the residuals between the estimated parameters and the theoretical results dictated by (2), i.e.,

$$\hat{\boldsymbol{p}}_{\mathrm{UE}} = \underset{\boldsymbol{p} \in \mathbb{R}^{2}}{\arg\min} \left(\|\boldsymbol{\theta}(\boldsymbol{p}_{\mathrm{BS}}, \boldsymbol{p}) - \hat{\theta}_{1}\| + \phi \|\boldsymbol{\tau}(\boldsymbol{p}_{\mathrm{BS}}, \boldsymbol{p}) - \hat{\tau}_{1}\| \right), \quad (6)$$

where $\phi>0$ is a regularization coefficient balancing the contribution of the AOA and the TOA components.

The two-stage formulation as in (6) facilitates localization in a manner that is invariant of the transmission scheme and waveform [15], [16]. The core challenge in (6) is thus in exploiting the diversity induced by the multi-band operation within FR3 to estimate the LOS AOA and TOA.

III. MULTI-FREQUENCY PARAMETERS ESTIMATION

In this section we propose a scheme for recovering θ_1, τ_1 from the FR3 observations in (5). As a preliminary step, we formulate a classical single sub-band beamformer scheme in Subsection III-A, which we extend into our multi-frequency multi-array FR3-tailored beamformer in Subsection III-B. Finally, we discuss its implications in Subsection III-C.

A. Single Sub-Band Beamformer

Localization by beamforming relies in the assumption that the noise and the underlying desired signal are uncorrelated, as is typically the case. In this subsection we formulate a single sub-band beamformer, thus the superscript $(\cdot)^{(k)}$ can be omitted. The details of such beamforming algorithm, which are reported below, are also summarized in Algorithm 1.

Localizing via beamforming is based on the spatial spectrum

$$P(\theta, \tau) = \frac{1}{T} \sum_{t=1}^{T} \left| (\boldsymbol{a}^{Q}(\tau))^{T} \boldsymbol{Y}_{t}^{H} \boldsymbol{a}^{M}(\theta) \right|. \tag{7}$$

The UE AOA-TOA pairs are the ones maximizing $P(\theta, \tau)$. This peak-finding involves searching over a 2D grid with steps sizes of $\Delta\theta$ and $\Delta\tau$:

$$\theta \in \{ -\frac{\pi}{2} \le i\Delta\theta \le \frac{\pi}{2} | i \in \mathbb{Z} \} \equiv \Theta$$

$$\tau \in \{ 0 \le j\Delta\tau \le \tau_{max} | j \in \mathbb{Z} \} \equiv \mathcal{T}.$$
(8)

Algorithm 2: FR3 Beamformer

Input: Multiple sub-bands samples $\{\{\boldsymbol{Y}_t\}_{t=1}^T\}_{k=1}^K$ Empirical threshold λ

Output: Estimated spectrum peak $(\hat{\theta}_1, \hat{\tau}_1)$

1 FR3 Beamformer

- calculate spectra $\{P^{(k)}(\theta,\tau)\}_{k=1}^K$ by (7)
- 3 filter noisy peaks \mathcal{X} by (10)
- 4 identify the peak $(\hat{\theta}_1, \hat{\tau}_1)$ by (11)
- 5 return $(\hat{\theta}_1, \hat{\tau}_1)$

The BS covers 180° , while the delay is bounded by the slot time $\tau_{max}=\frac{Q}{B}$. Accordingly, the parameters are recovered as

$$(\hat{\theta}_1, \hat{\tau}_1) = \underset{(\theta, \tau) \in \Theta \times \mathcal{T}}{\arg \max} P(\theta, \tau), \tag{9}$$

from which the UE's position is recovered via (2).

B. FR3 Beamformer

The classical beamformer in Algorithm 1 is tailored for a single sub-band, and is unable to capitalize on information from multiple sub-bands. The sub-bands in FR3 frequencies reveal different location information due to the different propagation characteristics and the difference in the number of antennas [10]. This motivates a new type of beamformer for FR3 that can reap benefits from its use of multiple diverse sub-bands with different arrays, coined *FR3 beamformer*.

Drawing inspiration from incoherent wideband processing schemes [21]–[23], the multi-frequency FR3 beamformer first estimates the spectrum peaks for each sub-band as in the single sub-band beamformer. Accordingly, we calculate the spatial spectra $\{P_k(\cdot,\cdot)\}$ by (7) (for each sub-band k) and the set of estimated peaks $(\hat{\theta}_1^{(k)}, \hat{\tau}_1^{(k)})$ by (9) for all sub-bands $k \in \{1,\ldots,K\}$. Each sub-band may detect different peaks, thus in general $\hat{\theta}_1^{(k_1)} \neq \hat{\theta}_1^{(k_2)}$ and $\hat{\tau}_1^{(k_1)} \neq \hat{\tau}_1^{(k_2)}$ for $k_1 \neq k_2$.

Note that the two-dimensional LOS peaks in different subbands may be below the noise level, resulting in the failure of detecting the LOS component as the global peak. Thus, the estimated peak values are filtered based on an empirical threshold value denoted $\lambda \geq 0$ that is set as a priori. Accordingly, the candidate peaks after this filtering are

$$\mathcal{X} = \{ (\hat{\theta}_1^{(k)}, \hat{\tau}_1^{(k)}) | P_k(\hat{\theta}_1^{(k)}, \hat{\tau}_1^{(k)}) > \lambda, \ \forall k \}.$$
 (10)

Among multiple peak values obtained after filtering from different sub-bands, we select the one that belongs to the highest frequency sub-band, i.e.,

$$(\hat{\theta}_1, \hat{\tau}_1) = \underset{(\hat{\theta}_1^{(k)}, \hat{\tau}_1^{(k)}) \in \mathcal{X}}{\arg \max} k. \tag{11}$$

The motivation for (11) stems from the fact that it has a high number of antenna elements that yields higher spatial resolutions. The entire algorithm is summarized in Algorithm 2.

C. Discussion

The core novelty of the FR3 beamforming scheme lies in the adaptivity to choose the most suitable sub-band. The lower sub-bands within FR3 have attractive propagation properties,

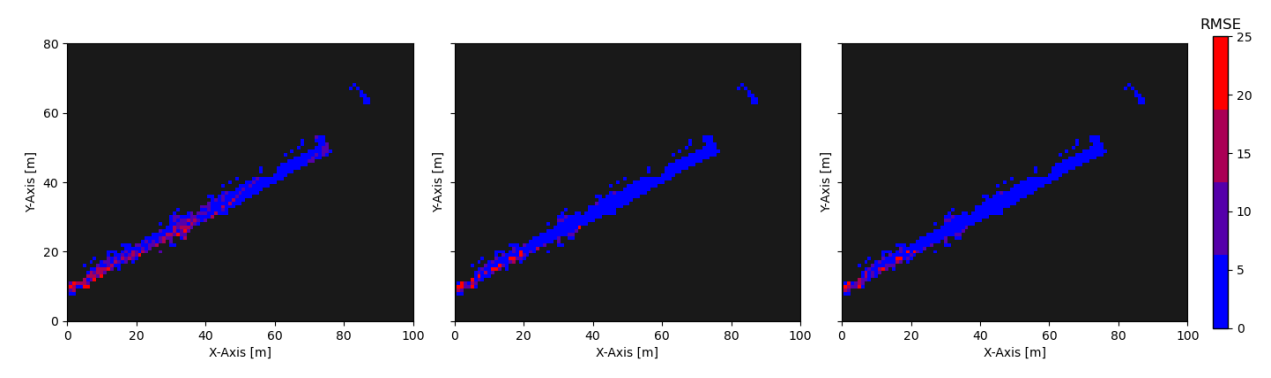


Fig. 2: Localization results: heatmaps illustrating the localization RMSE for each link. Left to right: (1) Left - 6 GHz, (2) Middle - 24 GHz, (3) Right - {6 GHz, 24 GHz}. The colorbar presents the encoding of the different RMSE ranges.

TABLE I: Simulation parameters.

| Parameters | | | Values | | |
|---|--------------|-------|-----------------|---------------|---------------|
| Area (m ²) | | | 100×70 | | |
| Noise power spectral density N_0 (dBm/Hz) | | | -174 | | |
| Noise figure (dB) | | | 7 | | |
| Number of UEs | | | 400 | | |
| Maximum number of multipaths | | | 25 | | |
| Empirical threshold λ | | | 1.2 | | |
| Frequency-dependent parameters | | | | | |
| Frequency [GHz] | 6 | 12 | | 18 | 24 |
| Bandwidth [MHz] | 6 | 12 | | 24 | 48 |
| BS ULA dimensions | 1×4 | 1 × 8 | | 1×16 | 1×24 |
| Subcarrier spacing [KHz] | 60 | 60 | | 120 | 240 |
| Subcarrier numbers | 100 | 200 | | 200 | 200 |

while the higher frequency sub-bands are preferable owing to the higher number of antennas and larger bandwidth. Doing so balances resilience to noise and multipath separability.

To formulate the time complexity of our FR3 beamformer, we note that Algorithm 1 requires $O(|\Theta| \cdot |\mathcal{T}| \cdot M \cdot Q)$ multiplications. Accordingly, our algorithm has $O(K \cdot |\Theta| \cdot |\mathcal{T}| \cdot M \cdot Q)$, as it employs Algorithm 1 K times followed by simple post-processing. It is noted that its excessive computational overhead can be mitigated by employing parallelization across the sub-bands using appropriate hardware. We design FR3 beamformer as a form of incoherent multi-band processing, combining information from each sub-band separately. while the fact that each sub-band is associated with a different ULA limits the applicability of conventional coherent multi-band processing, which jointly processes the received signals from multiple, one can consider machine learning to combine the sub-bands, as was recently shown to facilitate multi-band array processing [24], [25].

IV. NUMERICAL RESULTS

To numerically evaluate our proposed scheme we use the data from [10], where extensive ray-tracing simulation was performed in a dense urban area (see Fig. 1). This data consists of channel parameters including the path-loss, delay, and AOA for each path. All simulation parameters are listed in Table I. In addition, the space of antenna element is half the wavelength $d^{(k)} = \frac{c}{2f^{(k)}}$ for the carrier frequency $f^{(k)}$. These values were chosen in accordance with the narrowband condition in [20], which states that $\pi M^{(k)} B^{(k)} \ll f^{(k)}$ must be satisfied. Our source code and data are available at [26].

Our first study considers using the two extreme frequencies 6 GHz and 24 GHz. For the beamformer, we use resolutions $\Delta\theta = 0.1^{\circ}$ and $\Delta\tau = 5$ ns. Localization error is measured as the average of RMSE [m] on all links. Fig 2 depicts multiple maps of the links with their respective RMSE, when the transmitted power is 20 dBm and the BS is positioned at [80, 60], for different configurations. In the 6GHz sub-band (left part of Fig 2), most links are resolvable. The non-separable links include locations that are in the medium-to-high range of the BS. In the 24 GHz (middle of Fig 2), more links could resolved in the higher distances due to the favorable characteristics of this sub-band. However, the non-resolvable links suffer from high RMSEs since the received power drops rapidly until it falls below the noise level, completely failing the localization of the UE in these instances. The multi-frequency FR3 beamformer utilizes the best of both sub-bands (right part of Fig. 2), correctly localizing both in near and far positions.

Next, we evaluate the average localization RMSE, computed over the 400 links, as a function of the transmitted power. We take all four sub-bands in Table I into account. In Fig 3, we can observe that when the transmitted power is above the noise level, each sub-band exhibits a different RMSE behavior, reaching a different error-floor. For the 24 GHz sub-band, the average RMSE error-floor is lower than in the 6 GHz subband as multipath components can be easily resolved with a larger number of antennas at 24 GHz. In addition, for 6 GHz, increasing the transmission power doesn't reduce the average RMSE as the number of antennas is insufficient to achieve a high spatial resolution. Note that our beamformer surpasses employing each individual sub-band, successfully choosing the highest angular-resolution peak when the power is -10dBm or above. Note that identical results (that were thus omitted) were obtained when using the 2-dimensional MUSIC spectrum [27] for the localization task, indicating that our approach can also be employed with alternative beamformers.

To further investigate error variations across sub-bands, we analyze the cumulative distribution function (CDF) of the RMSE using a transmitted power of 30 dBm, as depicted in Fig. 4. These curves indicate that the 24 GHz sub-band resolves the majority of links when power exceeds noise levels. Specifically, localization using this sub-band achieves an RMSE below 10 m for 95% of links. Notably, employing a

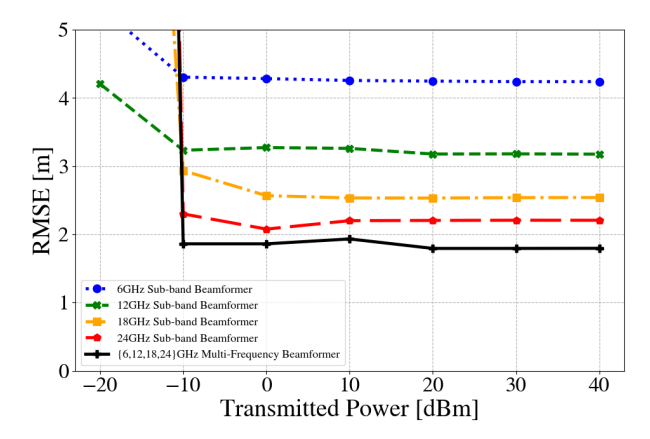


Fig. 3: Curves depicting the average localization RMSE as a function of the transmitted power. The multi-frequency FR3 beamformer exploits additional sub-bands, resulting in the lowest RMSE among the depicted baselines.

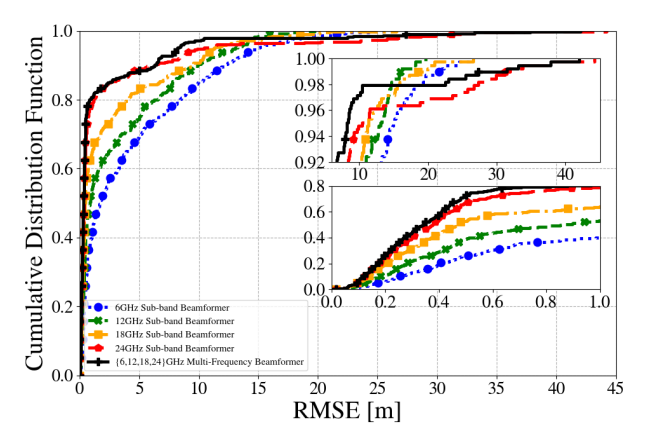


Fig. 4: Empirical cumulative distribution function of the RMSE using a fixed transmitted power of 30 dBm.

combination of 6 GHz, 24 GHz sub-bands increases this ratio to 96%, and utilizing all four sub-bands further improves it to 98%. Nonetheless, for the remaining 2% of links, i.e. 8 links in our dataset, the selection rule fails to choose the low RMSE peaks in the lower sub-bands, resulting in noisy 24 GHz outputs. This underscores the potential improvement of the selection algorithm that currently relies on a global λ threshold. For example, one could adapt this threshold for each link leveraging machine learning.

V. CONCLUSIONS

We introduced a localization method that is designed to leverage the spatial and spectral diversity provided by the FR3 band. Our proposed beamformer exploits information from its multiple sub-bands to reduce the overall localization error rate. We evaluated its gains in a cellular urban scenario via ray-tracing simulations of densely clustered areas.

REFERENCES

- Z. Qadir, K. N. Le, N. Saeed, and H. S. Munawar, "Towards 6G internet of things: Recent advances, use cases, and open challenges," *ICT Express*, vol. 9, no. 3, pp. 296–312, 2023.
- [2] A. Faisal, M. Kamruzzaman, T. Yigitcanlar, and G. Currie, "Understanding autonomous vehicles," *Journal of Transport and Land Use*, vol. 12, no. 1, pp. 45–72, 2019.

- [3] J. He, K. Yang, and H.-H. Chen, "6G cellular networks and connected autonomous vehicles," *IEEE Netw.*, vol. 35, no. 4, pp. 255–261, 2020.
- [4] H. Wymeersch and G. Seco-Granados, "Radio localization and sensing—part I: Fundamentals," *IEEE Commun. Lett.*, vol. 26, no. 12, pp. 2816–2820, 2022.
- [5] H. Wymeersch, G. Seco-Granados, G. Destino, D. Dardari, and F. Tufvesson, "5G mmWave positioning for vehicular networks," *IEEE Wireless Commun.*, vol. 24, no. 6, pp. 80–86, 2017.
- [6] H.-J. Song and N. Lee, "Terahertz communications: Challenges in the next decade," *IEEE Trans. THz Sci. Technol.*, vol. 12, pp. 105–117, 2021.
- [7] K. Du, O. Ozdemir, F. Erden, and I. Guvenc, "Sub-terahertz and mmwave penetration loss measurements for indoor environments," in *IEEE ICC Workshops*, 2021.
- [8] L. Dai, J. Tan, Z. Chen, and H. V. Poor, "Delay-phase precoding for wideband THz massive MIMO," *IEEE Trans. Wireless Commun.*, vol. 21, no. 9, pp. 7271–7286, 2022.
- [9] M. Ma, N. T. Nguyen, and M. Juntti, "Beam squint analysis and mitigation via hybrid beamforming design in THz communications," in *Proc. IEEE ICC*, 2023, pp. 6486–6491.
- [10] S. Kang, M. Mezzavilla, S. Rangan, A. Madanayake, S. B. Venkatakrishnan, G. Hellbourg, M. Ghosh, H. Rahmani, and A. Dhananjay, "Cellular wireless networks in the upper mid-band," *IEEE Open J. Commun. Soc*, vol. 5, pp. 2058–2075, 2024.
- [11] Z. Cui, P. Zhang, and S. Pollin, "6G wireless communications in 7-24 GHz band: Opportunities, techniques, and challenges," *arXiv preprint* arXiv:2310.06425, 2023.
- [12] K. Lee, J. Kim, E. W. Jin, and K. S. Kim, "Extreme massive MIMO for upper-mid band 6G communications," in *Proc. IEEE ICTC*, 2022, pp. 997–999
- [13] S. Kang, G. Geraci, M. Mezzavilla, and S. Rangan, "Terrestrial-satellite spectrum sharing in the upper mid-band with interference nulling," arXiv preprint arXiv:2311.12965, 2023.
- [14] L. Italiano, B. C. Tedeschini, M. Brambilla, H. Huang, M. Nicoli, and H. Wymeersch, "A tutorial on 5G positioning," arXiv preprint arXiv:2311.10551, 2023.
- [15] N. Garcia, H. Wymeersch, E. G. Larsson, A. M. Haimovich, and M. Coulon, "Direct localization for massive MIMO," *IEEE Trans. Signal Process.*, vol. 65, no. 10, pp. 2475–2487, 2017.
- [16] W. Fan, S. Liu, C. Li, and Y. Huang, "Fast direct localization for millimeter wave MIMO systems via deep ADMM unfolding," *IEEE Wireless Commun. Lett.*, vol. 12, no. 4, pp. 748–752, 2023.
- [17] J. Tuta and M. B. Juric, "MFAM: multiple frequency adaptive model-based indoor localization method," Sensors, vol. 18, no. 4, p. 963, 2018.
- [18] M. A. Skoglund, G. Hendeby, J. Nygårds, J. Rantakokko, and G. Eriksson, "Indoor localization using multi-frequency RSS," in *Proc. IEEE/ION PLANS*, 2016, pp. 789–798.
- [19] T. Kazaz, G. J. Janssen, J. Romme, and A.-J. Van der Veen, "Delay estimation for ranging and localization using multiband channel state information," *IEEE Trans. Wireless Commun.*, vol. 21, no. 4, pp. 2591– 2607, 2021.
- [20] S. Weng, F. Jiang, and H. Wymeersch, "Wideband mmwave massive MIMO channel estimation and localization," *IEEE Wireless Commun. Lett.*, vol. 12, no. 8, pp. 1314–1318, 2023.
- [21] M. Wax, T.-J. Shan, and T. Kailath, "Spatio-temporal spectral analysis by eigenstructure methods," *IEEE Trans. Acoust., Speech, Signal Process.*, vol. 32, no. 4, pp. 817–827, 1984.
- [22] S. Chandran and M. Ibrahim, "DoA estimation of wide-band signals based on time-frequency analysis," *IEEE J. Ocean. Eng.*, vol. 24, no. 1, pp. 116–121, 1999.
- [23] S. Argentieri and P. Danes, "Broadband variations of the MUSIC highresolution method for sound source localization in robotics," in *Proc. IEEE/RSJ IROS*, 2007, pp. 2009–2014.
- [24] J. P. Merkofer, G. Revach, N. Shlezinger, T. Routtenberg, and R. J. van Sloun, "DA-MUSIC: Data-driven DoA estimation via deep augmented MUSIC algorithm," *IEEE Trans. Veh. Technol.*, vol. 73, no. 2, pp. 2771– 2785, 2023.
- [25] D. H. Shmuel, J. P. Merkofer, G. Revach, R. J. van Sloun, and N. Shlezinger, "SubspaceNet: Deep learning-aided subspace methods for DoA estimation," arXiv preprint arXiv:2306.02271, 2023.
- [26] "Upper mid-band localization git hub repository," https://github.com/ tomerraviv95/higher-mid-bands-localization, available on-line.
- [27] R. Schmidt, "Multiple emitter location and signal parameter estimation," IEEE Trans. Antennas Propag., vol. 34, no. 3, pp. 276–280, 1986.